Magnetite-rutile symplectite derived from ilmenite-hematite solid solution in the Xinjie Fe-Ti oxide-bearing, mafic-ultramafic layered intrusion (SW China)

Wei Tan[1,2], Christina Yan Wang[1], Hongping He[1,3,*], Changming Xing[1], Xiaoliang Liang[1,3] and Huan Dong[1,2]

[1]CAS Key Laboratory of Mineralogy and Metallogeny, Guangzhou Institute of Geochemistry, Chinese Academy of Sciences, Guangzhou 510640, China
[2]University of Chinese Academy of Sciences, Beijing 100049, China
[3]Guangdong Provincial Key Laboratory of Mineral Physics and Materials, Guangzhou 510640, China

Abstract

A unique symplectitic intergrowth of magnetite + rutile is hosted by ilmenite in the gabbro of the Xinjie Fe-Ti oxide-bearing, mafic-ultramafic layered intrusion. The crystallization of rutile in the symplectite is probably formed by oxidation of ilmenite-hematite solid solution (Ilm-Hem$_{ss}$). Segregation of Fe^{3+} in the Ilm-Hem$_{ss}$ at the rutile-host interfaces triggered the crystallization of magnetite along the margin of the growing rutile, and shaped the vermicular morphology of the rutile. The crystallization of magnetite can also locally release Ti^{4+} to enhance the progressive growth and subsequent nucleation of rutile in the symplectite. The growth of the symplectite ceased when the temperature decreased to that of the miscibility gap of Ilm-Hem$_{ss}$ and Fe^{3+} began to exsolve to form hematite lamellae in the ilmenite.

Keywords: Magnetite-rutile symplectite, solid transformation, ilmenite-hematite solid solution, hematite lamellae

Introduction

Both hematite (Fe_2O_3) and ilmenite ($FeTiO_3$) are rhombohedral and can form a complete solid-solution series (Ilm-Hem$_{ss}$) above ~650 °C (Lindsley 1991). A miscibility gap would separate a hematite-rich phase from an ilmenite-rich phase on cooling. Therefore, hematite lamellae that have thicknesses ranging from tens of micrometers to the nanoscale are commonly observed in the ilmenites of many Fe-Ti oxide-bearing layered intrusions (McEnroe et al. 2002; Robinson et al. 2002; Kasama et al. 2009). An assemblage of magnetite + rutile is supposed to be more stable than, or at least thermodynamically equal to, an assemblage of ilmenite + hematite (Lindsley 1991). However, the assemblage of magnetite + rutile is seldom observed in rocks, especially plutons. It is also difficult to obtain satisfactory experimental results on the equilibrium of magnetite + rutile and ilmenite + hematite assemblages due to the slow reaction rates of the Ilm-Hem$_{ss}$ system (Frost 1991; Lindsley 1991).

Symplectites of magnetite/ilmenite + pyroxene, clinopyroxene/olivine + plagioclase (± hornblende ± quartz) and quartz + plagioclase are well documented, and several mechanisms have been proposed to explain their genesis (Moseley 1984; Hippertt and Valarelli 1998; Field 2008; Dégi et al. 2010; Elardo et al. 2012). In this study, we observed a symplectite of magnetite + rutile in close intergrowth with an assemblage of ilmenite host + hematite lamellae in the gabbro of the Xinjie layered intrusion (SW China). This special intergrowth is ideal to investigate the factors that control the solid transformation of Ilm-Hem$_{ss}$. The unusual occurrence of magnetite + rutile symplectite may also

have an important bearing on the variation of physicochemical conditions during the evolution of a layered intrusion.

Sampling and methods

The Xinjie intrusion is one of the Fe-Ti oxide-bearing, mafic-ultramafic layered intrusions in the Panxi region in SW China (map available[1]). These intrusions are part of the Emeishan Large Igneous Province, which is believed to be formed from a mantle plume at ~260 Ma (Chung and Jahn 1995). The Xinjie intrusion consists of distinct mineral assemblages: from the base upward, a marginal zone and three Units (I, II, and III) (Wang et al. 2008; Dong et al. 2013). The section in which the ilmenite hosts a symplectite of magnetite + rutile (Fig. 1a) occurs at the bottom of Fe-Ti oxide-rich layers in Unit III.

The backscattered electron (BSE) images and compositions of minerals were obtained on polished thin sections by using a JEOL-JXA8230 electron microprobe analyzer (EMPA). The micro-X-ray diffraction analyses were conducted on a Rigaku D/max Rapis IIR micro-XRD system at 40 kV and 250 mA (Cu$K\alpha$) with exposures of 20–60 min. The X-ray beam is ~100 μm in diameter and was focused on the selected spots on the thin sections. Raman spectra were obtained on a RM2000 laser Raman spectrometer by employing 514.5 nm line of Ar ion laser.
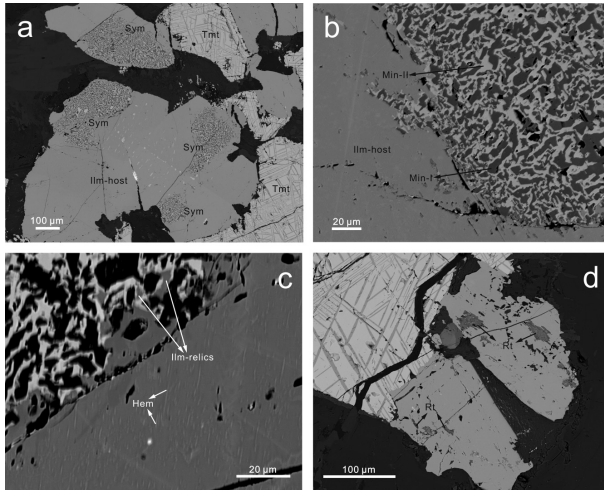
Results

The symplectite of magnetite + rutile is myrmekite-like, and occurs within or in the margin of ilmenite grains (Fig. 1a). The symplectite is composed of vermicular rutile (Min-I) and interstitial magnetite (Min-II) (Fig. 1b). Min-I is rimmed by Min-II and the whole symplectite is serrated in the boundary with ilmenite. Relics of ilmenite occasionally occur within or along the boundary of the symplectite (Fig. 1c).

Min-I exhibits Raman bands indicative of rutile at ca. 238, 445, and 611 cm^{-1} (Glass and Fries 2008), whereas Min-II exhib-

---

FIGURE 1. BSE images of symplectite-bearing ilmenite in the Xinjie intrusion. (**a**) Irregular symplectite (Sym) in host ilmenite (Ilm). (**b**) Symplectite composed of vermicular Min-I (dark gray, rutile) and interstitial Min-II (white, magnetite). (**c**) Ilmenite relics in the symplectite and ultrafine hematite (Hem) lamellae in host ilmenite. (**d**) Ilmenite exsolves irregular rutile (Rt).

FIGURE 2. Raman spectra of Min-I (Rutile) and Min-II (Magnetite) in the symplectite (see Fig. 1b), and the ilmenite host with hematite (Hem) exsolution (see Fig. 1c).

its those of magnetite at ca. 310, 546, and 671 cm^{-1} (Shebanova and Lazor 2003) (Figs. 2a and 2b). The symplectite exhibits intensive peaks of rutile and magnetite on the micro-XRD patterns (Fig. 3a). The cell parameters of rutile are $a_0 = 4.5904(4)$ and $c_0 = 2.9569(5)$ Å, and that of magnetite is $a_0 = 8.3947(8)$ Å. Min-I (rutile) contains ~2.6 wt% FeO and Min-II (magnetite) contains ~3.9 wt% TiO$_2$ (Table 1).

The host ilmenite of the symplectite contains 6–11 wt% Fe$_2$O$_3$ (Table 1). The host ilmenite exhibits nanoscale lamellae in the

TABLE 1. EMPA of the symplectite and the host mineral (in wt%)

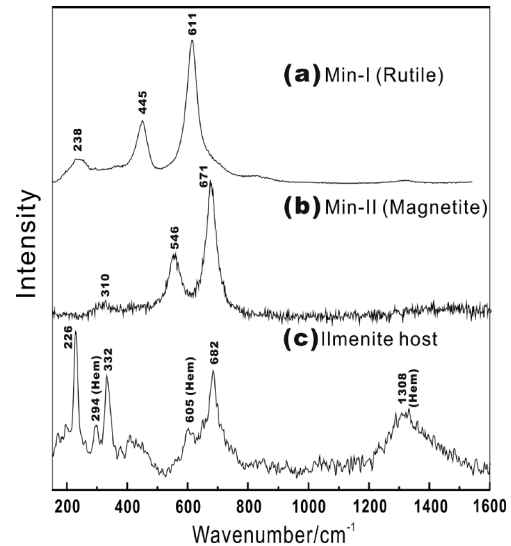| Element (wt%)	Min-I (rutile)		Min-II (magnetite)		Mass-balance calculation[a]		Host ilmenite (Ilm-Hem$_{ss}$ precursor)	
	Avg	St.dev.	Avg	St.dev.	Avg	St.dev.	Avg	St.dev.
	(n = 6)		(n = 7)		(n = 3)		(n = 8)	
SiO$_2$	0.01	–	0.04	–	0.03	–	0.01	–
MgO	0.02	–	0.01	–	0.02	–	0.34	–
Al$_2$O$_3$	0.01	–	0.01	–	0.01	–	–	–
FeO[b]	2.63	0.73	34.74	0.70	22.14	0.70	42.54	0.63
Fe$_2$O$_3$[b]	–	–	61.36	1.36	37.28	1.33	8.45	1.32
MnO	–	–	0.01	–	0.01	–	0.66	–
NiO	–	–	0.06	–	0.04	–	0.02	–
Cr$_2$O$_3$	0.01	–	0.02	–	0.02	–	0.01	–
TiO$_2$	97.12	0.98	3.90	0.70	40.48	2.02	48.70	0.70
Total	99.81	0.33	100.15	0.62	100.02	0.01	100.73	0.20
	% of image area[c]							
(n = 3)	44.0	2.5	56.0	2.5				
	Normalized wt%							
(n = 3)	39.2	2.2	60.8	2.2				
ΣFe/Ti[d]					1.53		1.14	

[a] The mass-balance calculation of the symplectite using the measured compositions of Min-I and Min-II in relative proportions determined by Model analysis of their areas in the BSE images (listed below the composition data).
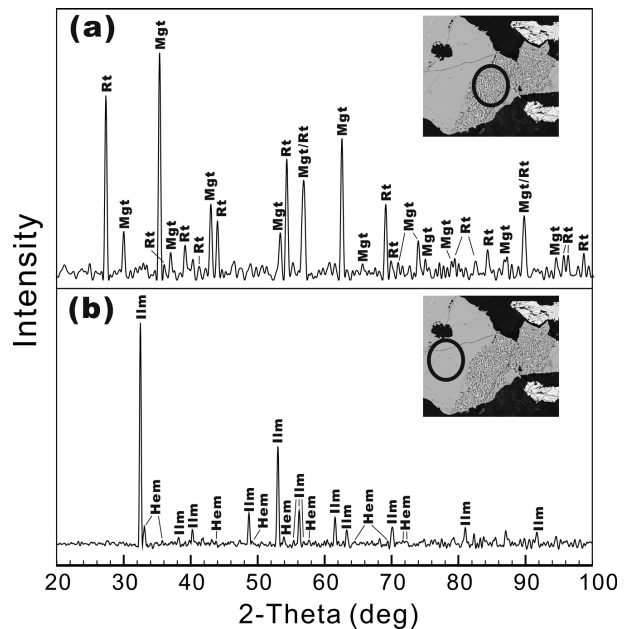[b] Redistribution of ΣFeO between Fe$_2$O$_3$ and FeO is on the basis of charge balance and stoichiometry of rutile, magnetite, and ilmenite, respectively.
[c] The image area percents of Min-I and Min-II in the symplectite were taken to be the same as volume percents.
[d] ΣFe/Ti = (Fe^{2+} + Fe^{3+})/Ti^{4+}.

FIGURE 3. XRD patterns adopted in situ on the symplectite of magnetite (Mgt) + rutile (Rt) and the host ilmenite with hematite (Hem) lamellae. The test area is shown by black circles.

high-contrast BSE images (Fig. 1c), which cannot be analyzed using EPMA. However, in addition to three Raman bands indicative of ilmenite at ca. 226, 332, and 682 cm^{-1} (Wang et al. 2004), the host ilmenite also shows three Raman bands that characterize hematite at ca. 430, 605, and 1370 cm^{-1} (Wang et al. 2004) (Fig. 2c). The host ilmenite also exhibits additional XRD reflections of hematite at ca. 2.70, 1.69, 1.59, 1.31, 1.19, 1.16, 1.14, 1.08, and 1.04 Å (Fig. 3b). The cell parameters of the host ilmenite are $a_0 = 5.088(2)$ and $c_0 = 14.092(7)$ Å, and those of hematite a_0

= 5.04(1) and c_0 = 13.77(2) Å, nearly identical to the values for stoichiometric compositions (Blake et al. 1966; Wechsler and Prewitt 1984). Therefore, we consider that the nanoscale lamellae in the host ilmenite are composed of hematite. The large standard deviation on the values for Fe_2O_3 content of the host ilmenite is thus attributed to the uneven distribution of hematite lamellae in the host ilmenite.
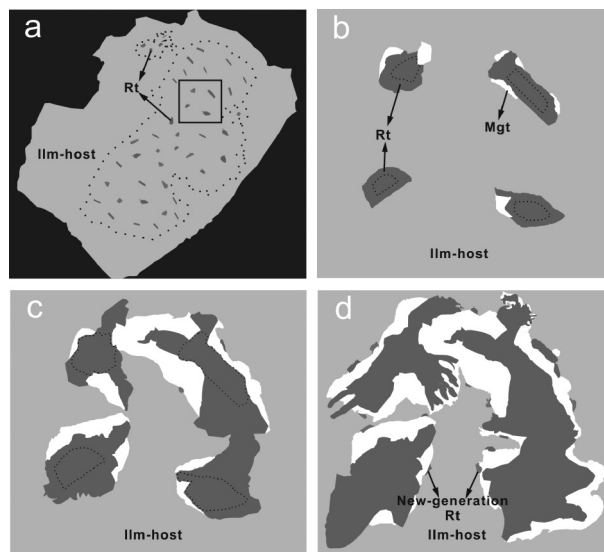
DISCUSSION

The Gibbs free energy change (ΔG_v) would provide a driving force to trigger the solid phase transformation of metastable minerals, whereas energy barriers would be generated by the interface energy change (ΔG_s) and the interface strain energy change (ΔG_ξ) (Trivedi 1970). In the case that the assemblage of magnetite + rutile is thermodynamically equal to the assemblage of hematite + ilmenite, the transformation from Ilm-Hem$_{ss}$ to each of the assemblages would have the same ΔG_v value. As both hematite and ilmenite belong to the trigonal system, they tend to form a coherent interface in solid transformation (Robinson et al. 2002); in contrast, rutile is tetragonal and magnetite cubic, so they tend to form an incoherent interface in solid transformation. In theory, a coherent interface has energy barrier ($\Delta G_s + \Delta G_\xi$) that is lower than that of an incoherent interface (Jiang and Lu 2008). Therefore, the assemblage of magnetite + rutile is much less commonly observed than hematite + ilmenite as the solid transformation product of Ilm-Hem$_{ss}$.

The host ilmenite of magnetite + rutile symplectite in the Xinjie intrusion has no reactive or replacement textures with adjacent minerals, ruling out the possibility that the symplectite of magnetite + rutile formed by reaction of the host ilmenite with interstitial fluids or adjacent minerals. This indicates that the symplectite probably transformed from a precursor. Note that the host ilmenite is in close coexistence with titanomagnetite (Fig. 1a), the magnetite + rutile symplectite is, thus, unlikely to have been derived from a pseudobrookite-ferropseudobrookite solid solution, which cannot coexist with magnetite-ulvöspinel solid solution in the TiO_2-FeO-Fe_2O_3 system (Mullen and Mccallum 2013). The bulk composition of the magnetite + rutile symplectite has ~22 wt% FeO, ~37 wt% Fe_2O_3, and ~40 wt% TiO_2, and a ΣFe/Ti ratio of 1.53 (Table 1). The bulk composition of the symplectite has much higher Fe^{3+} and ΣFe/Ti ratio than that of the ilmenite that hosts the hematite lamellae. We consider that the original Ilm-Hem$_{ss}$ may have experienced sub-solidus oxidation to produce a more Fe-rich Ilm-Hem$_{ss}$, as shown by the reaction:

$$Fe_2O_3 \cdot 5FeTiO_{3(Ti\text{-}rich\ Ilm\text{-}Hem\ ss)} + O_2 =$$
$$3Fe_2O_3 \cdot FeTiO_{3(Ti\text{-}poor\ Ilm\text{-}Hem\ ss)} + 4TiO_2.$$

The reaction has been proved by both natural and experimental observation (Lindsley 1963; Southwick 1968). The oxidation process also leads to heterogeneous nucleation of rutile within the ilmenite, which is consistent with the appearance of rutile exsolution in the ilmenite in the Xinjie intrusion (Fig. 1d).

We consider that the nucleation of rutile probably plays a key role in the formation of the symplectite of magnetite + rutile. The early-exsolved, fine rutile crystals served as crystal seeds (Fig. 4a), and may keep coarsening on cooling (Cacciuto et al. 2004). The growth of rutile would consume Ti^{4+} and generate excess Fe^{2+}

FIGURE 4. Schematic diagram illustrating the formation process of the magnetite (Mgt) + rutile (Rt) symplectite. (**a**) Exsolution of fine-grained rutile. (**b**) A close-up of **a**, showing the crystallization of magnetite at the interface between the ilmenite host and the exsolved rutile. (**c**) The random growth of rutile with coarsening of adjacent magnetite. (**d**) Nucleation of the "new-generation" rutile and onset of a new symplectite growth cycle.

along the Ilm-Hem$_{ss}$ boundary. The rutile exsolution also results in elastic strain relaxation and additional dislocations along the boundary, so that the Fe^{3+} in the Ilm-Hem$_{ss}$ would have a greater chemical potential to diffuse toward the boundary (Hondros and Seah 1977). With the segregation of Fe^{3+} and accumulation of Fe^{2+}, magnetite tends to nucleate and grow up along the interface between the ilmenite host and exsolved rutile (Fig. 4b). Note that the magnetite crystallization around the rutile is observed along the boundary of the symplectite (Figs. 1b and 1c). The parts where the rutile is rimmed by magnetite precipitation would stop growing, whereas the other parts free from magnetite would continue to grow. This may explain the vermicular morphology of the rutile (Fig. 4c). Progressive segregation of Fe^{3+} enhanced the growth of magnetite, which, in turn, consumed Fe^{2+} and released excess Ti^{4+} in the Ilm-Hem$_{ss}$. Magnetite can also act as a "barrier" and hinder the diffusion of Ti^{4+} toward the growing rutile, so that Ti^{4+} would accumulate to form a new generation of rutile along the interface between the magnetite and the ilmenite host (Fig. 4d), triggering a new growth cycle of the symplectite.

Progressive consumption of Fe^{3+} would weaken the driving force for the cyclic growth of the symplectite so that the late-stage symplectite is smaller and coexists with relics of primary ilmenite (Fig. 1b). The cyclic growth of the symplectite would terminate at temperatures < ~650 °C, and Fe^{3+} would exsolve to form hematite lamellae within host ilmenite.

IMPLICATIONS

Ilm-Hem$_{ss}$ is sensitive to the changes in temperature, oxygen fugacity, and chemical composition of the original melts, so that even subtle component variance in the Ilm-Hem$_{ss}$ can be well reflected by the features of its exsolution/decomposition products.

We ascribed the formation of magnetite + rutile symplectite to sub-solidus oxidation of Ilm-Hem$_{ss}$ under relatively oxidizing conditions, which are controlled by the composition and proportion of interstitial fluids (Buddington and Lindsley 1964). The layers of Units I and II in the Xinjie intrusion mainly contain Ti-rich ilmenite intergrown with rutile and sphene, whereas the layers of Unit III contain both titanomagnetite and ilmenite with magnetite/hematite lamellae. It seems that the Fe-Ti oxides in Unit III crystallized at higher f_{O_2} than those in Unit I and II. The elevated f_{O_2} may also be related to an increase in the proportion of interstitial fluids. Therefore, the ilmenite hosting the magnetite-rutile symplectite may serve as a typomorphic mineral to partition petrographic layers formed under different f_{O_2}.

ACKNOWLEDGMENTS

REFERENCES CITED

Blake, R.L., Hessevic, R.E., Zoltai, T., and Finger, L.W. (1966) Refinement of hematite structure. American Mineralogist, 51, 123–129.

Buddington, A.F., and Lindsley, D.H. (1964) Iron-titanium oxide minerals and synthetic equivalents. Journal of Petrology, 5, 310–357.

Cacciuto, A., Auer, S., and Frenkel, D. (2004) Onset of heterogeneous crystal nucleation in colloidal suspensions. Nature, 428, 404–406.

Chung, S.L., and Jahn, B.M. (1995) Plume-lithosphere interaction in generation of the Emeishan flood basalts at the Permian-Triassic boundary. Geology, 23, 889–892.

Dégi, J., Abart, R., Török, K., Bali, E., Wirth, R., and Rhede, D. (2010) Symplectite formation during decompression induced garnet breakdown in lower crustal mafic granulite xenoliths: mechanisms and rates. Contributions to Mineralogy and Petrology, 159, 293–314.

Dong, H., Xing, C.M., and Wang, C.Y. (2013) Textures and mineral compositions of the Xinjie layered intrusion, SW China: Implications for the origin of magnetite and fractionation process of Fe-Ti-rich basaltic magmas. Geoscience Frontiers, 4, 503–515.

Elardo, S.M., McCubbin, F.M., and Shearer, C.K. (2012) Chromite symplectites in Mg-suite troctolite 76535 as evidence for infiltration metasomatism of a lunar layered intrusion. Geochimica et Cosmochimica Acta, 87, 154–177.

Field, S.W. (2008) Diffusion, discontinuous precipitation, metamorphism, and metasomatism: The complex history of South African upper-mantle symplectites. American Mineralogist, 93, 618–631.

Frost, B.R. (1991) Stability of oxide minerals in metamorphic rocks. Reviews in Mineralogy and Geochemistry, 25, 469–488.

Glass, B.P., and Fries, M. (2008) Micro-Raman spectroscopic study of fine-grained, shock-metamorphosed rock fragments from the Australasian microtektite layer. Meteoritics & Planetary Science, 43, 1487–1496.

Hippertt, J.F., and Valarelli, J.V. (1998) Myrmekite: Constraints on the available models and a new hypothesis for its formation. European Journal of Mineralogy, 10, 317–331.

Hondros, E., and Seah, M. (1977) Segregation to interfaces. International Metals Reviews, 22, 262–301.

Jiang, Q., and Lu, H. (2008) Size dependent interface energy and its applications. Surface Science Reports, 63, 427–464.

Kasama, T., Dunin-Borkowski, R.E., Asaka, T., Harrison, R.J., Chong, R.K., McEnroe, S.A., Simpson, E.T., Matsui, Y., and Putnis, A. (2009) The application of Lorentz transmission electron microscopy to the study of lamellar magnetism in hematite-ilmenite. American Mineralogist, 94, 262–269.

Lindsley, D.H. (1963) Fe–Ti oxides in rocks as thermometers and oxygen barometers. Carnegie Institute of Washington Yearbook, 62, 60–66.

——— (1991) Experimental studies of oxide minerals. Reviews in Mineralogy and Geochemistry, 25, 69–106.

McEnroe, S., Harrison, R., Robinson, P., and Langenhorst, F. (2002) Nanoscale haematite–ilmenite lamellae in massive ilmenite rock: an example of 'lamellar magnetism' with implications for planetary magnetic anomalies. Geophysical Journal International, 151, 890–912.

Moseley, D. (1984) Symplectic exsolution in olivine. American Mineralogist, 69, 139–153.

Mullen, E.K., and Mccallum, I.S. (2013) Coexisting pseudobrookite, ilmenite, and titanomagnetite in hornblende andesite of the Coleman Pinnacle flow, Mount Baker, Washington: Evidence for a highly oxidized arc magma. American Mineralogist, 98, 417–425.

Robinson, P., Harrison, R.J., McEnroe, S.A., and Hargraves, R.B. (2002) Lamellar magnetism in the haematite–ilmenite series as an explanation for strong remanent magnetization. Nature, 418, 517–520.

Shebanova, O.N., and Lazor, P. (2003) Raman study of magnetite (Fe$_3$O$_4$): Laser-induced thermal effects and oxidation. Journal of Raman Spectroscopy, 34, 845–852.

Southwick, D.L. (1968) Mineralogy of a rutile- and apatite-bearing ultramafic chlorite rock, Harford county, Maryland. Geological Survey Research, 600-C, 38–44.

Trivedi, R. (1970) The role of interfacial free energy and interface kinetics during the growth of precipitate plates and needles. Metallurgical Transactions, 1, 921–927.

Wang, A., Kuebler, K.E., Jolliff, B.L., and Haskin, L.A. (2004) Raman spectroscopy of Fe-Ti-Cr-oxides, case study: martian meteorite EETA79001. American Mineralogist, 89, 665–680.

Wang, C.Y., Zhou, M.F., and Zhao, D.G. (2008) Fe-Ti-Cr oxides from the Permian Xinjie mafic-ultramafic layered intrusion in the Emeishan large igneous province, SW China: Crystallization from Fe- and Ti-rich basaltic magmas. Lithos, 102, 198–217.

Wechsler, B.A., and Prewitt, C.T. (1984) Crystal structure of ilmenite (FeTiO$_3$) at high temperature and at high pressure. American Mineralogist, 69, 176–185.